buildings

MDPI

Article

Reuse of Solid Bricks in Construction: An Experimental Work

Erion Luga [1], Enea Mustafaraj [1], Emrah Tasdemir [1], Marco Corradi [2,*], Ervis Lika [3] and Erion Periku [4]

[1] College of Engineering and Technology, American University of the Middle East, Egaila 54200, Kuwait; erion.luga@aum.edu.kw (E.L.); enea.mustafaraj@aum.edu.kw (E.M.); emrah.tasdemir@aum.edu.kw (E.T.)
[2] Department of Engineering and Technology, University of Huddersfield, Huddersfield HD1 3DH, UK
[3] Risi Construction Company, 2001 Durres, Albania; construction.risi@gmail.com
[4] Independent Researcher, 1023 Tirana, Albania; erionperiku@gmail.com
* Correspondence: m.corradi@hud.ac.uk; Tel.: +44-1484-422-288

Abstract

This study experimentally and numerically examines the structural and seismic performance of recycled solid-brick masonry infills and load-bearing walls constructed from demolition materials. Solid bricks recovered from demolished structures were reused as infill in reinforced concrete (RC) frames and as standalone walls. Five full-scale panels, bare, 50% infilled, and 100% infilled frames, were tested under diagonal compression in accordance with ASTM E519-17, simulating in-plane seismic loading. Results showed that fully infilled frames exhibited a 149% increase in diagonal shear strength but a 40% reduction in ductility relative to the bare frame, indicating a trade-off between stiffness and deformation capacity. Finite element simulations using the Concrete Damaged Plasticity (CDP) model reproduced the experimental load–displacement curves with close agreement (within 6–8% in peak load) and captured the main failure patterns. Reusing cleaned demolition bricks reduces the demand for new fired bricks and helps divert construction waste from landfill, contributing to sustainable and circular construction. The findings confirm the potential of recycled masonry for low-carbon and seismic-resilient construction, provided that ductility limitations are appropriately addressed in design.

Keywords: recycled solid bricks; shear walls; reinforced concrete frames; new construction; finite element modeling; ductility and strength

check for updates

Academic Editor: Daniel Ferrández Vega

Received: 28 September 2025
Revised: 14 October 2025
Accepted: 27 October 2025
Published: 31 October 2025

Citation: Luga, E.; Mustafaraj, E.; Tasdemir, E.; Corradi, M.; Lika, E.; Periku, E. Reuse of Solid Bricks in Construction: An Experimental Work. *Buildings* **2025**, *15*, 3935. https://doi.org/10.3390/buildings15213935

Copyright: © 2025 by the authors. Licensee MDPI, Basel, Switzerland. This article is an open access article distributed under the terms and conditions of the Creative Commons Attribution (CC BY) license (https://creativecommons.org/licenses/by/4.0/).

1. Introduction

The demolition of old brickwork structures, often due to building abandonment, an aging population, or natural disasters, has generated a substantial amount of brick waste, which typically requires energy-intensive processing for crushing and reuse [1,2]. However, these bricks can be repurposed in various ways for new construction, either as load-bearing walls or as infill walls in Reinforced Concrete (RC) structures [3]. Since historic constructions were built using lime mortar, the removal of this relatively weak material is straightforward, allowing old solid bricks to be cleaned and reused effectively in new building projects. However, in most cases, bricks recycled from old buildings are crushed and not reused intact, except for some aesthetic purposes in projects aiming to replicate ancient walls. It is known, however, that old fired bricks often possess superior mechanical properties compared to modern ones produced through automated extrusion processes, which do not allow time for clay to settle. In contrast, traditional fired bricks were manufactured according to well-established historical methods that spanned several years from clay extraction to firing and final use. Moreover, the processes for eliminating

impurities from the clay were more thorough in the past, resulting in a higher-quality final product [4].

Masonry infill walls, although not specifically designed for load-bearing, contribute to the lateral stiffness and load-bearing capacity of RC frames. However, they also pose challenges, such as the potential for brittle failure during earthquakes [5,6]. Existing research on the seismic behavior of masonry infills in RC frames, while confirming that infill walls increase lateral strength and stiffness, also highlights trade-offs, particularly in reduced ductility and the risk of brittle failure [7,8]. Despite these challenges, over the years, several innovative techniques have been developed to enhance the seismic performance of masonry infill walls, ensuring that they contribute more effectively to the structural resilience of RC frames. One such technique is the use of expanded steel plates bonded to the infill walls, which allows the infill walls to carry a greater portion of the load during seismic events, reducing overall structural damage [9]. Another widely researched approach involves the retrofitting of damaged RC frames with Engineered Cementitious Composites (ECC) and Carbon Fiber-Reinforced Polymers (CFRP), which can enhance both compressive strength and load-carrying capacity. This technique has also shown improvements in energy dissipation, reducing the risk of collapse during seismic events [10–12].

In addition to retrofitting, Resilient Infill Walls (RIW), which incorporate gaps and metal connectors, has been shown to reduce initial stiffness while slowing down strength deterioration, thus improving the overall deformability and reducing damage [13]. Another promising development is the Damped Masonry Infilled Walls (DMIW), which features a novel Damping Layer Joint (DLJ) inserted within the infill, improving both the in-plane and out-of-plane seismic responses [14]. These advancements in infill wall technologies, along with design strategies such as symmetrically distributed infill walls [15] and the use of steel honeycomb structural fuses, significantly enhance load-bearing capacity, reduce drift, and improve seismic resilience in RC frames [16].

The influence of infill walls on the seismic capacity of RC buildings has been the subject of extensive research, with numerous studies proposing different materials and configurations to enhance structural performance. Stazi et al. [17] conducted experimental investigations of cross-laminated timber (CLT) infill walls, demonstrating their potential to improve seismic behavior. Furtado et al. [18] proposed retrofit strategies employing composite materials to mitigate cracking and damage in infill walls, thereby increasing resilience. Ricci et al. [19] conducted theoretical studies exploring the complex interaction between masonry infill walls and RC frames, highlighting the significant role these elements play in overall seismic response.

Another sustainable and more economical approach to this challenge is the use of recycled solid bricks for new infill walls. This study explores how solid clay bricks, sourced from demolished buildings, can be repurposed as a new construction material to improve both structural resilience and sustainability. By integrating recycled masonry, the study not only addresses the need for stronger, more durable construction but also contributes to reducing construction waste, promoting a circular economy. This dual focus on enhancing seismic performance and minimizing environmental impact positions recycled masonry as a practical and sustainable solution for urban infrastructure challenges.

To achieve this goal, both experimental testing and Finite Element Analysis (FEA) were employed to evaluate the structural performance of shear solid and infill walls. Experimental tests assess the load-bearing capacity and deformation characteristics of the walls, while FEA provides a detailed simulation of the frame-infill interaction under seismic conditions. Previous FEA studies, such as those by [6,20], have demonstrated the

effectiveness of numerical analysis in predicting complex behaviors, such as cracking and shear, providing a solid foundation for the modeling used in this research.

While previous studies have explored crushed brick aggregates and recycled masonry powders, the direct reuse of intact or slightly damaged solid bricks as infill within reinforced concrete frames remains scarcely investigated. This study addresses this gap by experimentally and numerically assessing the mechanical performance, seismic behavior, and sustainability implications of such infills. Recycled masonry offers a viable solution that reduces construction waste and helps cities meet their sustainability goals. These findings are particularly relevant for earthquake-prone regions, where improving building resilience can significantly reduce the risk of damage and expedite recovery in post-disaster scenarios.

2. Materials and Methods

The objective of this study is to investigate the reuse of clay solid bricks obtained from demolished masonry buildings. The reuse of pre-used solid bricks is uncommon and raises concerns about their mechanical performance. These bricks are often partially damaged or incomplete, making structural engineers hesitant to incorporate them into new masonry constructions or as infill walls in RC structures. The experimental campaign involved the preparation, construction, and diagonal compression testing of solid walls and RC frames with 0% (bare frame), 50%, 100% masonry infills, RC frame with aluminum frame infill, and a solid brick masonry load-bearing wall, while the FE modeling provided a deeper understanding of the frame-infill interaction under applied loading conditions.

2.1. Experimental Program

The experimental program focused on assessing the structural performance of recycled solid clay bricks. The materials used in this study include not only pre-used clay bricks, but also concrete, steel rebars, and traditional cement mortar. Testing procedures were conducted in accordance with international standards to ensure accuracy and reproducibility.

An experimental setup was developed to conduct laboratory experiments. The diagonal compression test setup, as per ASTM E519-17 [21], consists of a 50-ton capacity hydraulic jack, a reaction steel frame anchored to the laboratory strong wall, two steel loading shoes, and two LVDTs for deformation measurement. The steel shoes were attached to the specimen corners to apply uniform compression along the diagonal and to transfer load evenly to the test frame. The hydraulic jack was positioned between the steel frame and the top steel shoe to apply a compressive load, as depicted in Figure 1. Two orthogonally mounted LVDTs recorded the vertical shortening (ΔV) and horizontal extension (ΔH) of the wall panel, from which the shear strain (γ) was computed using the relationships defined in the standard. The resulting shear stress-strain response therefore represents the direct transformation of the measured load-displacement data, enabling accurate comparison with other masonry systems tested under the same protocol.

The measured mechanical parameters, such as shear stress, S_s, shearing strain, γ_s, and shear modulus, G, are calculated below:

$$S_s = \frac{0.707P}{A_n} \tag{1}$$

$$A_n = \frac{w+h}{2} t \cdot n \tag{2}$$

$$\gamma_s = \frac{\Delta V + \Delta H}{g} \tag{3}$$

$$G_{10} = \frac{(S_s)_{10kN}}{\gamma_S} \qquad G_{20} = \frac{(S_s)_{20kN}}{\gamma_S} \tag{4}$$

$$\mu = \frac{\mu_x + \mu_y}{2} \qquad \mu_x = \frac{\Delta f_x}{\Delta y_x} \qquad \mu_y = \frac{\Delta f_y}{\Delta y_y} \tag{5}$$

In Equations (1)–(5), P denotes the applied diagonal load (kN); A_n is the net sectional area (mm^2); w, h, and t represent the specimen's width, height, and thickness; n is the percent of the gross area of the unit that is solid; S_s denotes the calculated shear stress (MPa); γ_s is the corresponding shear strain; ΔV is the vertical shortening (mm); ΔH the horizontal extension; g the vertical gage length.

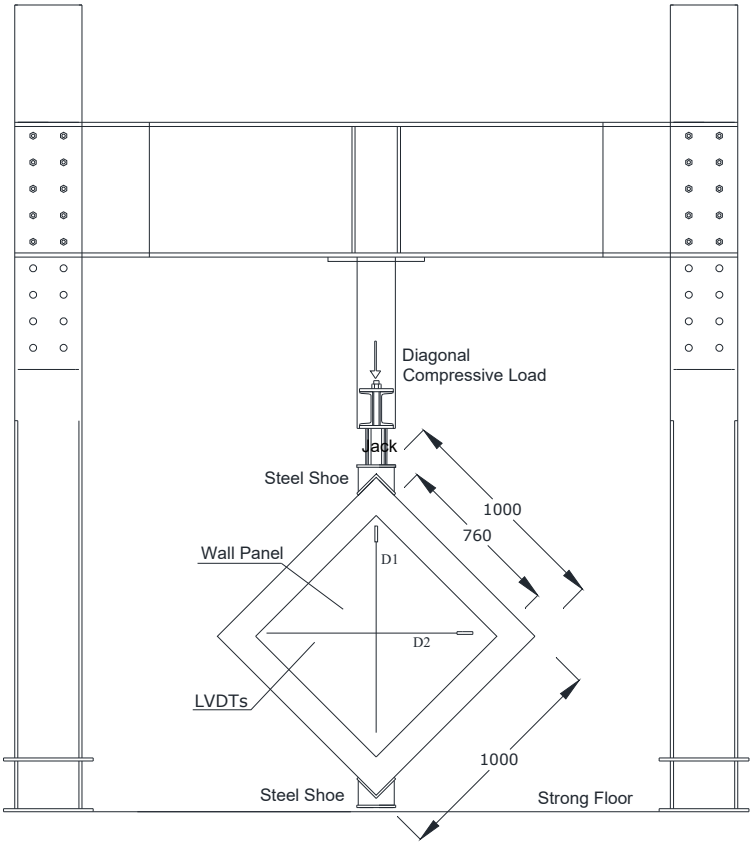

Figure 1. Diagonal compression test setup in accordance with ASTM E519-17: The hydraulic jack is positioned vertically on top of the upper steel shoe to apply compression along the wall's diagonal. The lower steel shoe rests on and is anchored to the strong floor. Two LVDTs (labeled D1 and D2) are installed along the wall diagonals to record deformations, including both shortenings and elongations (all units in mm).

Regarding wall stiffness, because the structural response in terms of stress and strain is highly nonlinear and non-elastic, it was decided to evaluate initial and secondary stiffness at two load levels (10 and 20 kN), both of which are typically below 50% of the failure load. The shear modulus was determined using Equation (4), defined as the slope of the secant line on the shear stress–strain curve, drawn from the origin through the stress points associated with the 10 kN and 20 kN loads.

Determination of the ductility of the wall panes was done using the deformation recordings from failure and yielding. The ductility factor was calculated from Equation (5), where Δf_x and Δf_y are the failure displacements in elongation and contraction, respectively, whereas Δy_x and Δy_y are the yielding deformations in each of the diagonals. The final ductility factor, μ, reported for each specimen corresponds to the average of the two diagonal measurements (μ_x and μ_y).

2.1.1. Design of Wall Specimens

In this experimental study, solid clay-fired bricks sourced from a single demolished building were used to construct both load-bearing brickwork wall and infill walls for RC structures. A total of five full-scale walls were built in the laboratory by the same bricklayer, using a consistent low-cement mortar mix. The RC frames were 1000 mm square specimens (external dimensions) and have a cross-sectional concrete area of 120 × 120 mm^2 (section A-A in Figure 2), reinforced with four longitudinal diameter (ϕ) 12 mm carbon steel rebars and stirrups of 6 mm placed at intervals of 50 or 100 mm (Figure 2). Concrete cover was 30 mm.

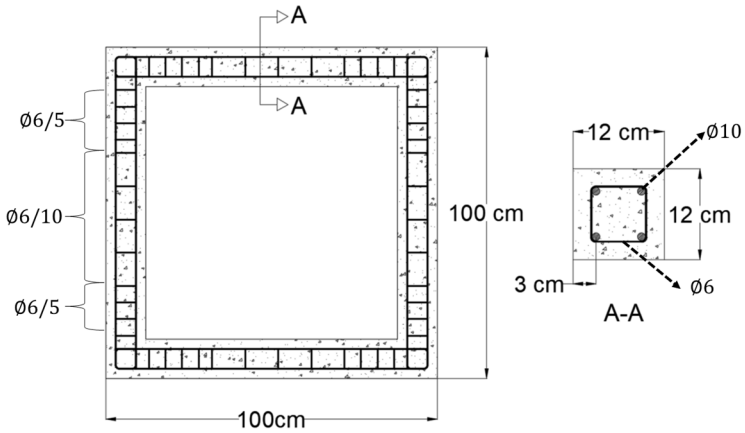

Figure 2. Reinforcement details of the RC frame.

The concrete used for the frames had a design strength of C25/30 (f_{ck} = 30 MPa), while B500C steel was used for reinforcement as per BS 4449 and EN 1992-1-1 [22,23]. RC frames were built in the laboratory. The concrete was poured into the formwork after the steel reinforcement was assembled. The curing process lasted 28 days before testing began (Figure 3). To ensure consistency, all frames were poured from the same batch of concrete. Compressive strength tests were performed on three cubic specimens (150 mm × 150 mm × 150 mm) in accordance with EN 206-1 [24].

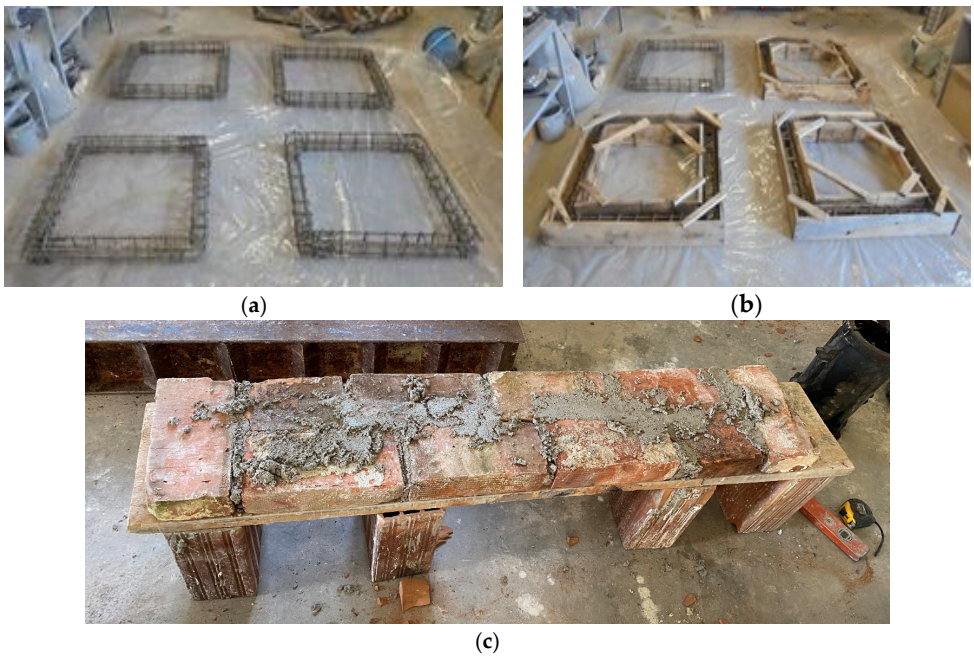

(**a**) (**b**)

(**c**)

Figure 3. (**a**) Steel reinforcement, (**b**) formwork, (**c**) building of the masonry wall.

2.1.2. Material Testing

The main mechanical properties of the construction materials were assessed individually prior to the diagonal compressive testing (Figure 4). The bricks used in the study were common solid clay bricks of 245 × 120 × 70 mm, retrieved from a demolished masonry structure. Bricks were subjected to flexural and compressive testing to assess their mechanical properties as per EN 771-1 [25]. The mortar used in this study for both load-bearing and infill walls was a traditional cement-lime mortar with a mix ratio of 1:1.5:6 (lime, cement, sand by volume). Mortar samples were cast in prismatic molds (40 × 40 × 160 mm) and cured for 28 days, after which flexural and compressive tests were conducted following EN 196-1 [26]. The average compressive strength of the mortar was recorded at 4.3 MPa, consistent with typical values used for masonry construction with a bed joint thickness of 15–20 mm [5]. The mechanical properties are listed in Table 1.

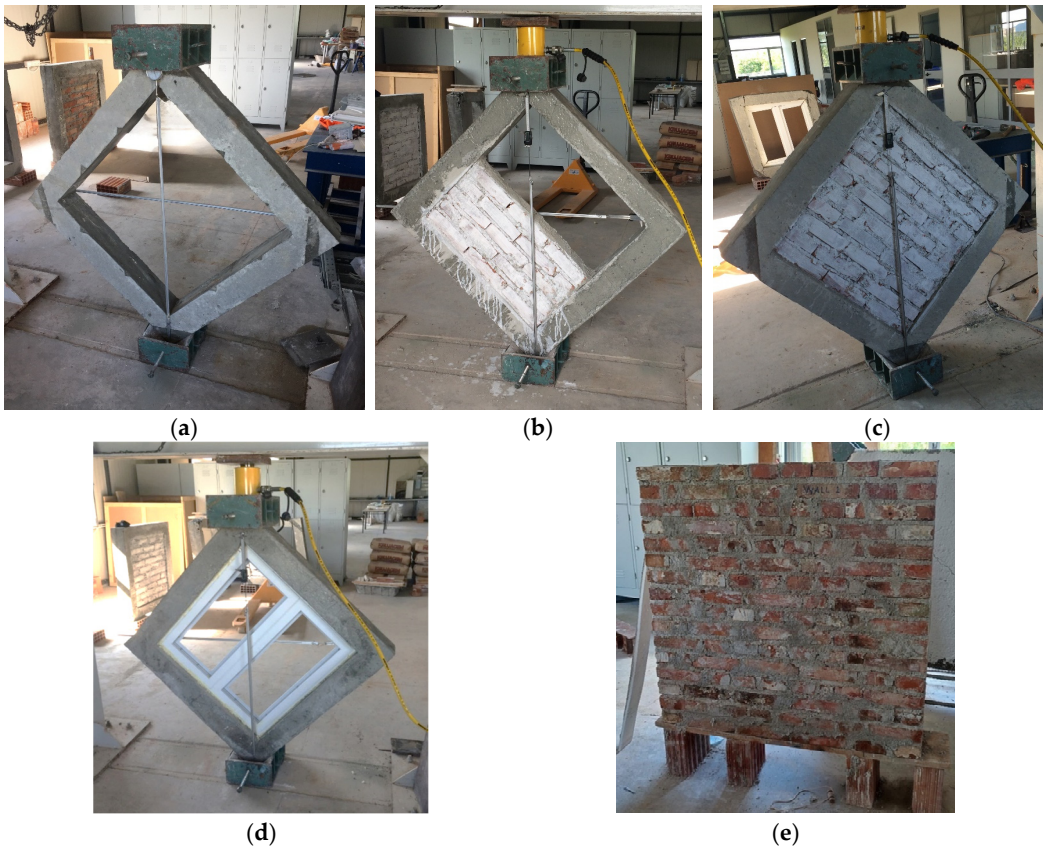

Figure 4. Concrete frames ready to be tested: (**a**) P1-00, 0% infill, (**b**) P2-50, 50% infill, (**c**) P3-100, 100% infill, (**d**) P4-Al, aluminum frame infill, and (**e**) P5-SB, solid brick masonry wall.

Table 1. Material test results, COV = Coefficients of Variation.

	Symbol	(MPa)	COV
Concrete compressive strength	f_{cc}	34.01	(0.21)
Reinforcing steel bar tensile strength	f_y	527	(0.07)
Steel reinforcement's ultimate strength	f_u	618	(0.05)
Solid brick compressive strength	f_{cb}	18.25	(0.25)
Solid brick flexural strength	f_{fb}	4.53	(0.33)
Mortar compressive strength	f_{cm}	4.3	(0.24)
Mortar flexural strength	f_{fm}	0.9	(0.13)
Masonry compressive strength	f_{cm}	14.01	(0.1)

2.1.3. Wall Panels and Testing

In this experimental campaign, five wall panels with different infill configurations were prepared and tested under diagonal compression, with one full-scale specimen per configuration due to the size and complexity of the setup. The mechanical properties of the constituent materials were determined from three replicate laboratory tests for each material type to ensure data reliability. Four were RC frames: one without infills (bare frame), one with 50% masonry infill, one with full (100%) masonry infill, and one with an aluminum window frame. In addition, a load-bearing masonry wall specimen (1200 × 1200 × 250 mm) was tested as a control, to compare the strength of the masonry alone with the structural behavior of the mixed RC–masonry panels. The infill was created by laying recycled clay solid bricks in a stretcher bond connected by a 15 mm thick mortar layer 14 days after the RC bare frame was cast. The frames were allowed to cure for an additional 28 days to ensure the mortar reached full strength. Once the concrete was cured, the specimens were tested in the test setup mentioned above by an incremental loading scheme until a failure mode was observed.

2.2. Finite Element Modeling

The finite element analysis was conducted using Abaqus [27] to simulate the behavior of RC frames with masonry infills under seismic loading. FEA provided deeper insights into the frame-infill interaction, which was challenging to capture entirely in the experimental tests due to material complexity.

Abaqus software was used to build the 3D finite element models of the tested specimens. An eight-node linear hexahedral solid element (C3D8R) with reduced integration and hourglass control was used to model both RC frames and expanded brick units. A two-node 3D truss element (T3D2) was used to model Steel members. The steel members were embedded in concrete elements with embedded tie constraints to simulate interaction. A structured mesh with mesh sizes of 30 mm and 20 mm was used for solid elements and steel elements, respectively. The load was applied as a displacement at the top of the frame. The translational movement (U_x, U_y, and U_z) of the top of the frame was restrained in the x and z directions, whereas it was released in the y direction. The boundary condition at the bottom of the frame was pinned. Figure 5 shows the element type, the boundary condition, and the experimental setup.

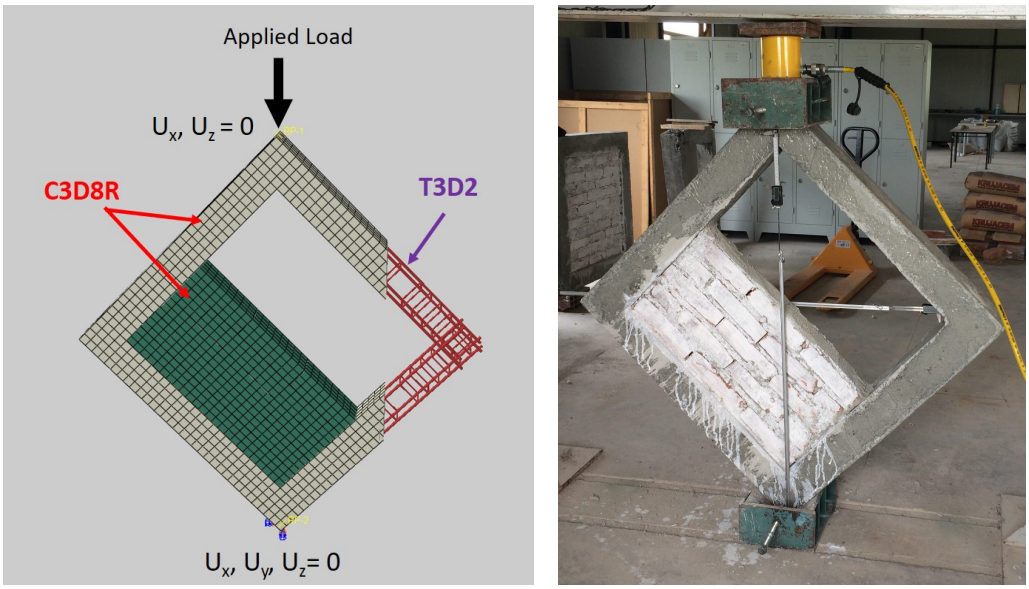

(**a**) (**b**)

Figure 5. (**a**) FE Model of the frame with 50% infill and (**b**) the corresponding experimental test.

As concrete and brick are not homogeneous materials, suitable modeling techniques are needed. The simplified micro-modeling technique was employed to simulate brick wall behavior [28]. The general contact algorithm with an all-self-contact domain was used to model the interaction between solid members [25]. The traction-separation law was utilized to model cohesive interaction for which a trial-and-error process was conducted to define initial stiffness values, which are K_{nn} = 20 MPa/mm, K_{ss} = 9 MPa/mm, and K_{tt} = 9 MPa/mm. The quadratic traction criterion with maximum nominal stresses of 0.23 MPa for the normal direction and 0.15 MPa for the tangential direction was used to model damage initiation. A displacement ratio (total/plastic) of 0.5 was used to specify a linear damage evolution. A penalty friction method with a coefficient of 0.75 was considered to model the post-damage frictional behavior, and hard contact was applied between the frame and masonry units sharing the boundary. The adopted mesh size accurately captured the force-transfer mechanisms at the concrete-brick interface, reproducing the experimental force-displacement response. Contact law parameters were adapted from the literature and refined for numerical stability, enabling faster convergence with the chosen mesh.

The Concrete Damaged Plasticity (CDP) model [29] was employed to model nonlinearity in concrete and masonry. The dilation angle (φ), equibiaxial-to-uniaxial strength ratio (f_b'/f_c'), yield surface shape factor (K_c), eccentricity (ε), and viscosity (μ) are key parameters needed for simulation. The dilation angle was set to 7°, whereas default values 1.16, 0.667, and 0.1 were used for f_b'/f_c', K_c, and ε, respectively. The viscosity parameter was taken to be 0.005 for both concrete and brick. The input stress–strain values used in the model, which were generated using software developed by Elkady [30], are shown in Figure 6. The average compressive strengths of the concrete and masonry units (brick and mortar), obtained experimentally, were 34.01 MPa and 14.01 MPa, respectively. The equivalent cylinder strength for the concrete material was taken as 80% of the cube strength, which is 27.21 MPa.

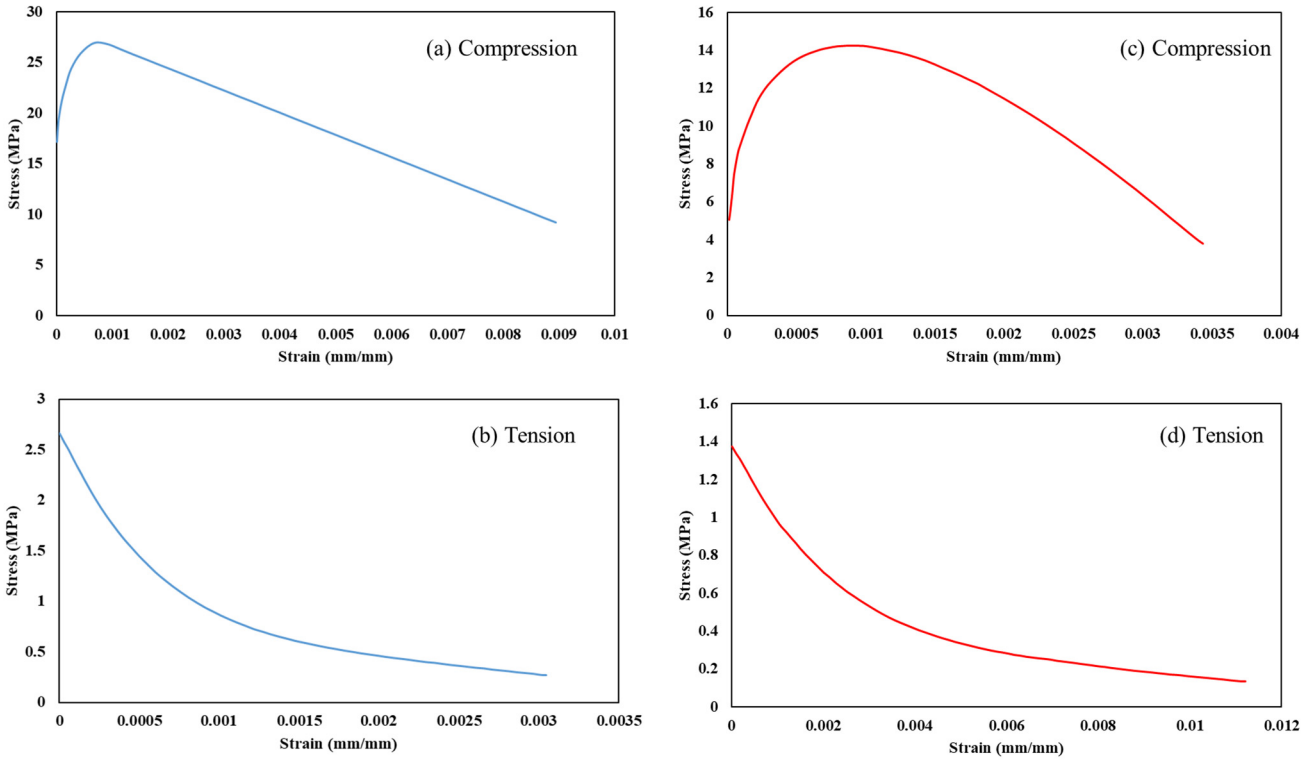

Figure 6. Stress–strain input parameters used in modeling: (**a**,**b**): concrete; (**c**,**d**): masonry.

Although the Concrete Damaged Plasticity (CDP) model was used, damage parameters were omitted to ensure smoother convergence. The plastic strain magnitude (PEMAG) [29] was instead employed to represent plastic deformation and structural damage; hence, damage parameters were excluded from Figure 6.

A bilinear stress-strain model was assigned to the steel reinforcement using isotropic hardening. The elastic range was defined with an elastic modulus of 200 GPa and a Poisson's ratio of 0.3, followed by plastic behavior initiated at the yield stress of 527 MPa.

3. Results and Discussion

This section presents a detailed analysis of the mechanical performance of the RC frames evaluated through experimental testing and finite element (FE) modeling. The main objective is to investigate how recycled masonry infills influence the structural properties of RC frames, including load-bearing capacity, ductility, and failure modes. The experimental findings highlight significant variations in strength and deformability between frames with 50% and 100% masonry infills and the bare frame, revealing a notable trade-off between increased strength and reduced ductility in infilled frames.

3.1. Experimental Results

The diagonal compression tests conducted on the frames aimed at load-bearing capacities, initial crack loads, maximum load capacities, and failure modes for each specimen. Observations reveal distinct load responses and deformation patterns, reflecting the impact of infill percentage on the frame's strength and ductility. Additionally, comparisons between experimental outcomes and finite element model predictions provide insights into the adequacy of recycled masonry infill as a strengthening material, highlighting its contributions to enhanced lateral stiffness and its implications for seismic resilience. The mechanical parameters of the tested frames are presented in Table 2.

Table 2. Diagonal compression test results.

	Wall Panel	P_{max} (kN)	S_s (MPa)	μ	G_{10} (MPa)	G_{20} (MPa)
P1-00	0% infill	45.0	0.265	8.66	39.3	14.1
P2-50	50% infill	47.5	0.280	4.96	153.7	76.8
P3-100	100% infill	112.1	0.590	5.03	392.8	196.4
P4-Al	aluminum frame infill	45.3	0.265	2.65	53.6	13.2
P5-SB	solid brick wall	39.9	0.094	1.01	71.0	39.5

The first experimental finding that emerges from the failure load values of the five wall panels is that the infill clay bricks had a significant influence on the in-plane capacity of the walls, as expected. The RC frame without infill (P1-00) failed at a diagonal load of 45 kN, whereas the fully infilled frame with solid clay bricks (P3-100) exhibited nearly a threefold increase, reaching a diagonal shear load of 112.1 kN. This observation is also consistent with the failure load of the wall panel composed entirely of solid bricks (P5-SB), which failed at a diagonal load of 39.9 kN.

If it is assumed that the two materials, the RC frame and the infill walls, begin resisting the diagonal load simultaneously and share it uniformly, then the combined resistance can be estimated by summing the failure load of the bare frame (45 kN) with that of P5-SB (39.9 kN), giving a total of 84.9 kN. This value is not significantly different from the experimentally measured failure load of P3-100.

Furthermore, the shear stiffness values G_{10} and G_{20} suggest that the solid brick walls (P5-SB) exhibit approximately twice the shear stiffness of the RC frame with infill during

the initial, more elastic, phase of diagonal in-plane loading. Consequently, the solid bricks are likely to carry a larger share of the diagonal shear load in the early loading stage. Only after the onset of cracking in the bricks, which leads to stiffness degradation, does the RC frame begin to absorb a greater proportion of the diagonal load.

The variability of the measured parameters was assessed through the coefficients of variation (COV) listed in Tables 1 and 2. These values, which range between 0.07 and 0.33 for the constituent materials and between 0.10 and 0.29 for the derived mechanical indices (G_{10}, G_{20}, μ), indicate an acceptable dispersion for laboratory-scale masonry testing. The limited number of full-scale specimens per configuration constrains the application of advanced variance modeling; however, the consistency between experimental and numerical results supports the reliability of the observed trends. Future work may employ replicate testing and statistical constitutive calibration, as suggested by [31], to further quantify the variability of the shear modulus and ductility.

Another noteworthy experimental observation concerns the effect of partial infill with solid bricks. In this study, a wall panel with 50% infill (P2-50) was tested under diagonal shear. The results indicate that partial infill does not provide a significant contribution to the shear resistance of the RC frame, which was an expected outcome. When only part of the frame's interior is filled with bricks, a continuous compressed diagonal strut cannot develop within the infill panel, leaving it largely unloaded and unable to contribute meaningfully to shear resistance. The experimental results confirmed this: the failure load of P1-50 wall (47.5 kN) was only slightly higher that the wall with 0 infill (45 kN, P1-00).

However, an unexpected result was observed regarding the shear stiffness. The shear stiffness G_{10} of the partially infilled wall (P2-50) increased to 153.7 MPa compared with 39.3 MPa for the bare RC frame (P1-00). While it is possible that the partial infill provided some confinement effect on the RC frame and reduced diagonal deformations under shear, it is more likely that this increase in stiffness resulted from natural variability in the properties of the materials used rather than from a genuine confinement effect of the partial infill.

Finally, the experimental results for the RC frame infilled with an aluminium commercial window frame (P4-Al) show, as expected, a structural response very similar to that of both the unfilled frame (P1-00) and the partially infilled frame (P2-50). The comparable failure load confirms that the aluminium window does not provide any significant contribution to the shear resistance of the frame and, like the partial infill, is unable to carry a significant share of the shear load. Specifically, Table 2 reports a failure load of 45.3 kN for P4-Al, compared with 45.0 kN for P1-00 and 47.5 kN for P2-50.

In this case, the shear modulus values further support this interpretation. The shear moduli G_{10} and G_{20} of P4-Al (53.6 MPa and 13.2 MPa, respectively) are essentially consistent with those of the unfilled frame (39.3 MPa and 14.1 MPa). This confirms that the aluminium window frame, due to both the low Young's modulus of aluminium and the very small cross-sectional area of the window elements, possesses negligible in-plane stiffness when subjected to diagonal loading.

In the P1-00 frame, the first crack appeared at 25 kN, with a displacement of 2.97 mm in compression and 5.36 mm in tension. The frame reached a maximum load of 45 kN before yielding. After yielding, the frame continued to deform plastically, with the steel reinforcement providing residual strength, as indicated by the elongation and compression values. The final displacement before failure was recorded as 55.12 mm in tension and 15.01 mm in compression (Figure 7). The crack pattern was mainly concentrated at the corners of the frame.

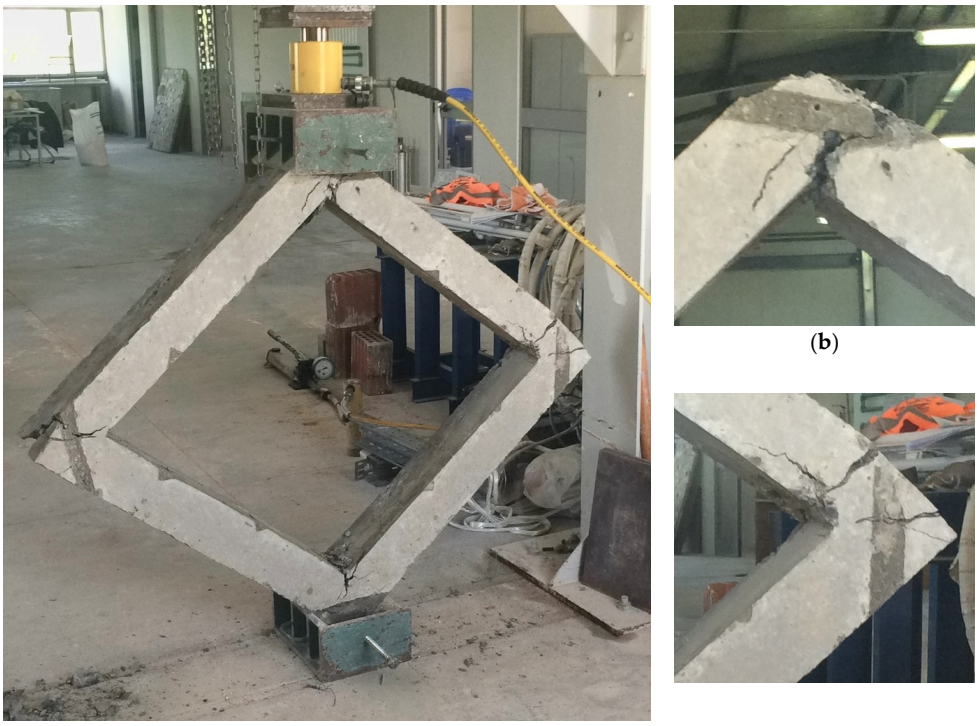

(**a**) (**b**) (**c**)

Figure 7. (**a**) Failure mode of the bare frame (0% infills); (**b**,**c**) Tension failure of concrete at the corners of the frame.

In P2-50 frame, the first crack occurred at a load of 40 kN, and the frame's maximum load capacity reached 47.5 kN. The maximum displacements were recorded at 27.99 mm in tension and 20.84 mm in compression before failure (Figure 8). As the load increased, the failure in the infill developed along the mortar joints. Similarly to the bare frame, the crushing of concrete around the four corners of the frame was observed. Compared to the bare frame, the 50% masonry infill improved the load-bearing capacity by just 5%, while also reducing the frame's overall ductility. This reduction in ductility is consistent with findings in other studies that note a trade-off between increased strength and reduced deformation capacity in masonry-infilled RC frames [32].

P3-100 frame exhibited the highest load-bearing capacity among the frames tested, with the initial crack occurring at a load of 80 kN and the frame reaching a maximum capacity of 112.1 kN. Displacements at failure were 53.80 mm in tension and 28.24 mm in compression (Figure 9). The 249% increase in strength is consistent with observations that full masonry infills significantly enhance load capacity but reduce ductility. This behavior indicates a trade-off that has been frequently reported, whereby increased strength from masonry infill corresponds with decreased deformation capacity, which can heighten the risk of brittle failure under cyclic seismic loads [33].

P4-Al frame exhibited a similar behavior as the bare frame P1-00. As expected, the aluminum frame did not have any subtle contribution to the load-carrying capacity of the frame. The first cracks on concrete occurred at a load of 26 kN, and the maximum load was recorded at 45.3 kN (Figure 10).

P5-SB specimen exhibited a diagonal compression failure, and the cracks appeared mainly on the mortar joints. The first crack occurred at a load of 33 kN, and at 39.9 kN the maximum load was reached. The failure was sudden, and the wall exhibited a brittle behavior (Figure 11).

Another parameter to assess the structural behavior of the frames was the shear stress–strain curve presented in Figure 12. As expected, P1-00 exhibited the lowest shear strength,

reaching a peak shear stress of 0.265 MPa. This is due to the absence of infill, which results in a lower lateral stiffness and capacity to resist applied shear forces. The inclusion of infill enhances the frame's shear strength, with the 50% infill case reaching a peak of 0.280 MPa and the 100% infill case peaking at around 0.590 MPa. This trend indicates that increasing the infill percentage leads to higher shear capacity, likely due to the enhanced load transfer and lateral stiffness that the infill provides. However, as previously reported, partial infill brick applications do not cause significant shear load capacity increments.

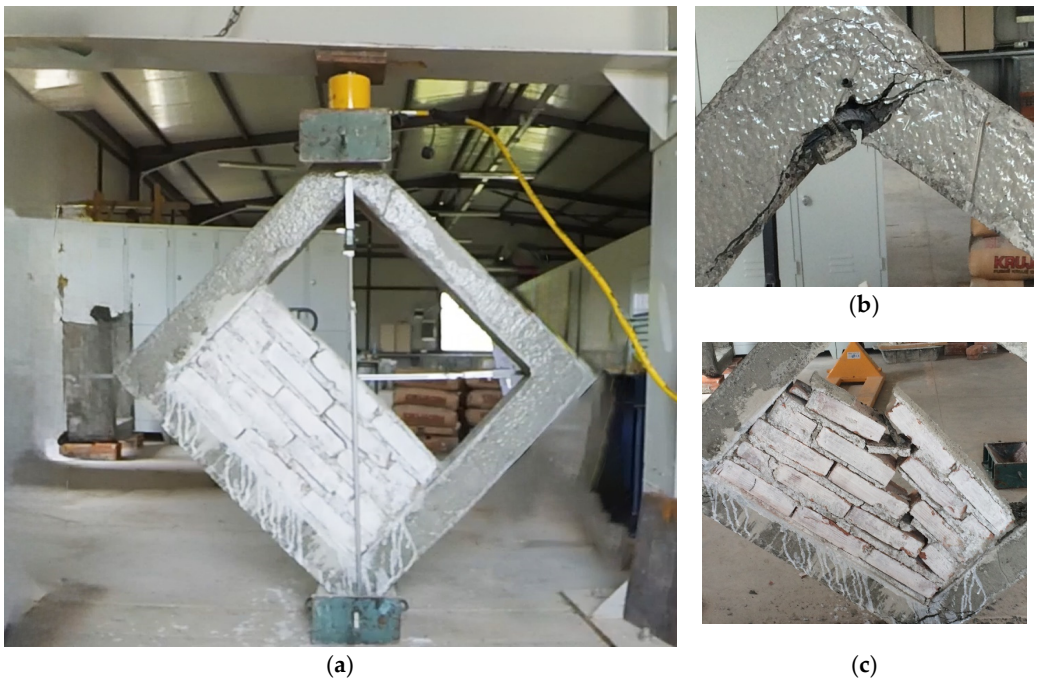

(**a**) (**b**) (**c**)

Figure 8. (**a**) Failure mode of the 50% infill frame, (**b**) tension failure of concrete at the corners of the frame, and (**c**) infill wall mortar cracking and debonding from bricks.

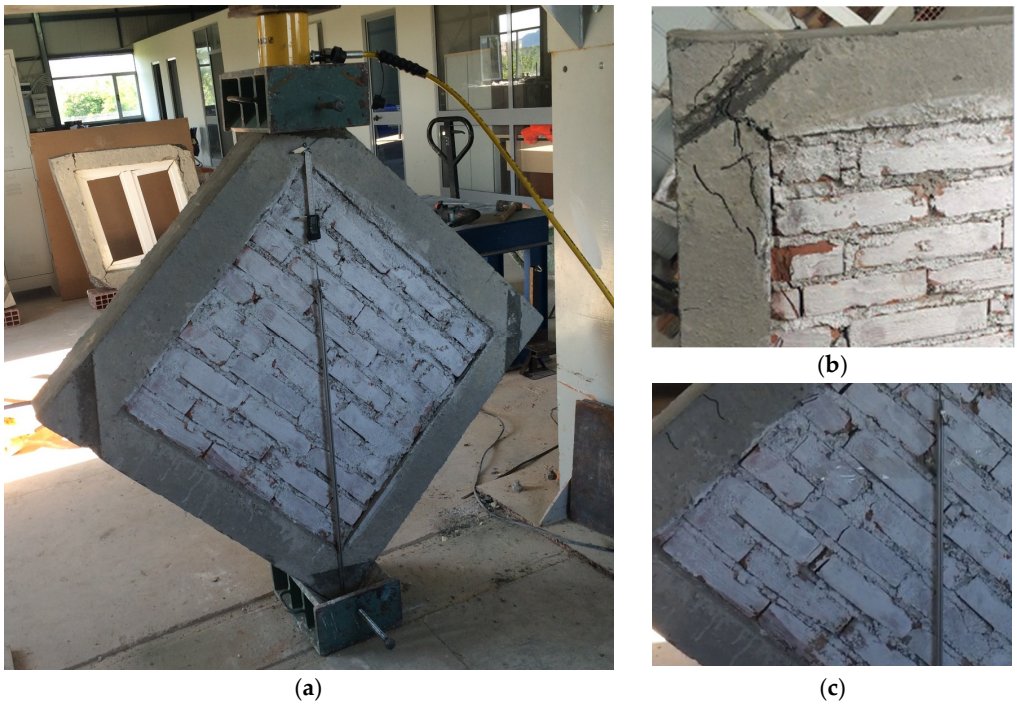

(**a**) (**b**) (**c**)

Figure 9. (**a**) 100% infill frame, (**b**) tension failure of concrete at the corners of the frame, and (**c**) infill wall mortar failure.



(**a**) (**b**) (**c**)

Figure 10. (**a**) Aluminum frame infill frame, (**b**,**c**) tension failure of concrete at the corners of the frame.

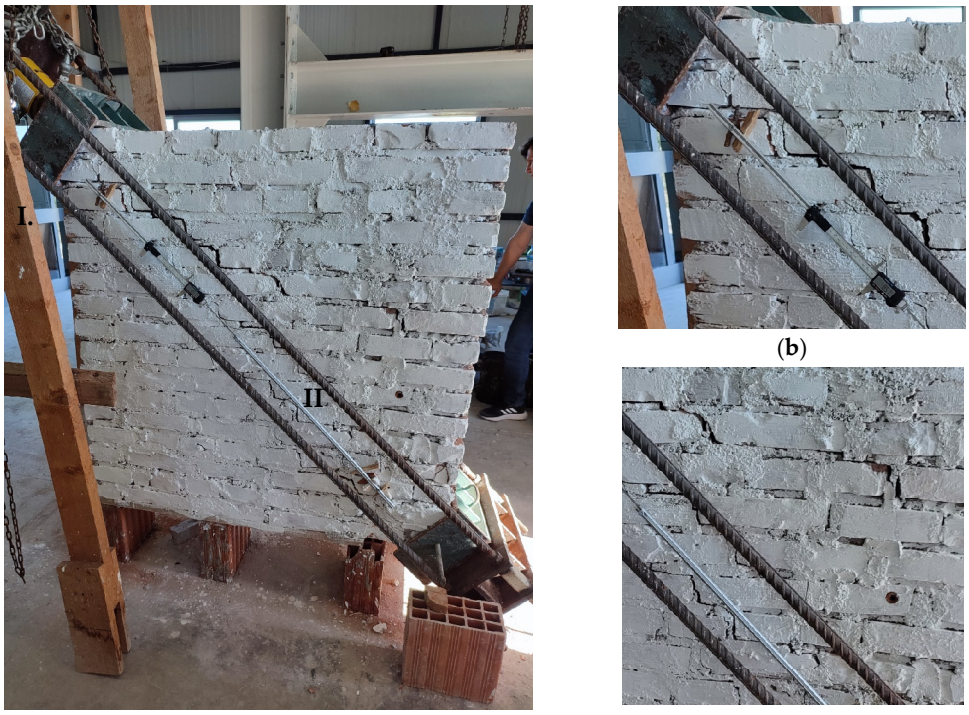

(**a**) (**b**) (**c**)

Figure 11. (**a**) the failure mode of the solid brick load-bearing wall, (**b**,**c**) diagonal step-like crack through mortar joints.

In addition to strength improvements, the infill also influences the ductility and post-peak behavior of the frame. The bare frame reaches its plateau in strain earlier and maintains a lower overall strain, indicating a ductile behavior but limited load-bearing capability. The 50% infill frame similarly reaches its strain plateau but shows slightly more resistance to

deformation than the bare frame. On the other hand, the 100% infill frame experiences a sharper initial increase in shear strain with increasing stress but plateaus at a lower strain level compared to the other frames, reflecting a stiffer response. This behavior suggests that the fully infilled frame deforms less and maintains structural integrity under higher stresses, which implies enhanced rigidity and reduced susceptibility to large deformations under load.

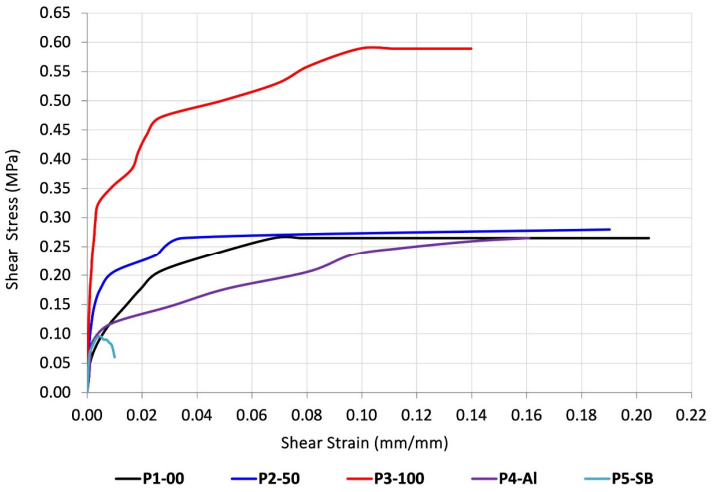

Figure 12. Experimental shear stress–strain diagram for all the tested specimens.

The stress–strain results are in line with the ductility coefficients obtained from Equation (5), where the bare frame, 50%, and 100% infill frames had an average factor of 8.66, 4.96, and 5.03, respectively (Table 2). These results align with existing literature, which suggests that masonry infills increase the stiffness and strength of RC frames but reduce their ductility, making them more prone to brittle failure under seismic loads [11,30]. This balance between strength and ductility is critical in designing RC frames for seismic applications, where both factors play a significant role in ensuring structural resilience.

The observed ≈149% increase in diagonal shear capacity and ≈40% reduction in ductility for fully infilled frames are consistent with recent literature. Grubišić et al. reported that adding clay-unit masonry infills to previously damaged RC frames increased initial stiffness and lateral strength and enhanced hysteretic damping, producing performance comparable to undamaged infilled frames under cyclic lateral loading [32]. Likewise, Kim et al. showed that construction precision and infill continuity strongly affect performance: the presence of a beam–wall gap reduced peak strength by 75–80% and stiffness by 55–70% relative to gap-free specimens, and thicker infills shifted failure toward column shear [31]. These external results align with our trends: continuous, well-engaged infills deliver large strength/stiffness gains but may reduce drift capacity, underscoring the importance of detailing and boundary conditions.

Additionally, the inverse correlation between strength and ductility has direct implications for seismic design. Fully infilled frames, though stronger, may concentrate damage in brittle diagonal cracking zones, leading to premature stiffness degradation. For moderate seismic regions, partial or discontinuous infills may provide a balance between stiffness and ductility.

3.2. FEM Results

The comparison between the FE model and the experimental results was conducted by analyzing both the load–displacement response and failure mode observations. The stress–strain curves for both the experiment and the FE model are shown in Figure 13. The initial stiffness of the model aligns well with the experimental data up to a displacement

of 2 mm, at which point a slight reduction in load occurs in the FE model due to the loss of bond between masonry units. After this sudden decrease, the load continues to increase, reaching peaks of 48, 50 and 120 kN for the bare frame, 50% infill, and 100% infill, respectively. This behavior is often observed when the material models do not fully capture the actual crack patterns. After reaching the maximum load in the FE model, the load fluctuations are also attributed to the sudden loss of bond between masonry units. Despite these differences, the FE model overall represents the force-displacement behavior of the experiment reasonably well. The analysis was terminated at 30 mm displacement due to a sudden load release, which caused significant instability and convergence issues in the model.

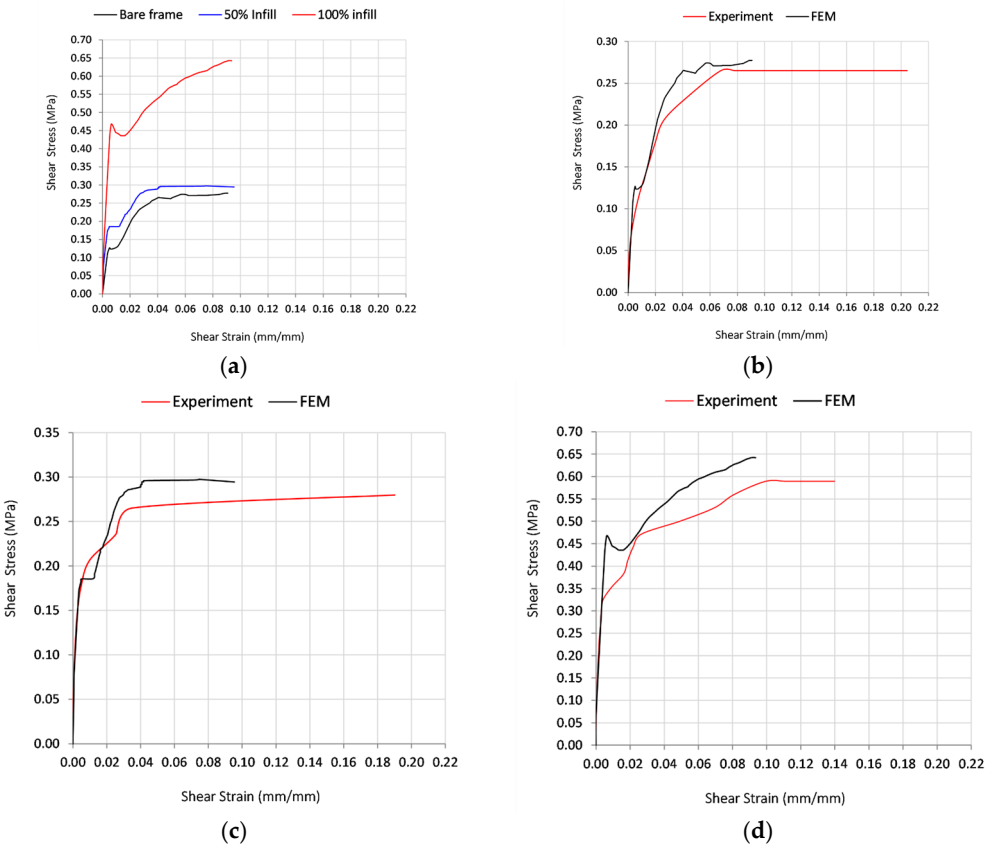

Figure 13. Comparison of the stress–strain results: (**a**) FEM results, (**b**) P1-00, 0% infill, (**c**) P2-50, 50% infill, (**d**) P3-100, 100% infill.

A strong correlation was observed between FE simulations and experimental observations of damage localization. As illustrated in Figure 14, plastic deformation, represented by the plastic strain magnitude (PEMAG) [29], was concentrated at the frame corners, consistent with the experimentally observed damage zones. However, cracking within the masonry units, clearly visible during testing, was not fully reproduced in the FE models. This limitation likely stems from the complex interaction among the mortar, masonry units, and reinforced concrete frame, as well as from the heterogeneous nature of the materials and the simplified representation of interfacial bonding through cohesive parameters. Additionally, geometric imperfections inherent to the recycled brick units could not be incorporated into the numerical model, which may have further affected the prediction of the crack pattern. Nevertheless, the FE models effectively captured the overall failure behavior of both the bare and infilled frames.

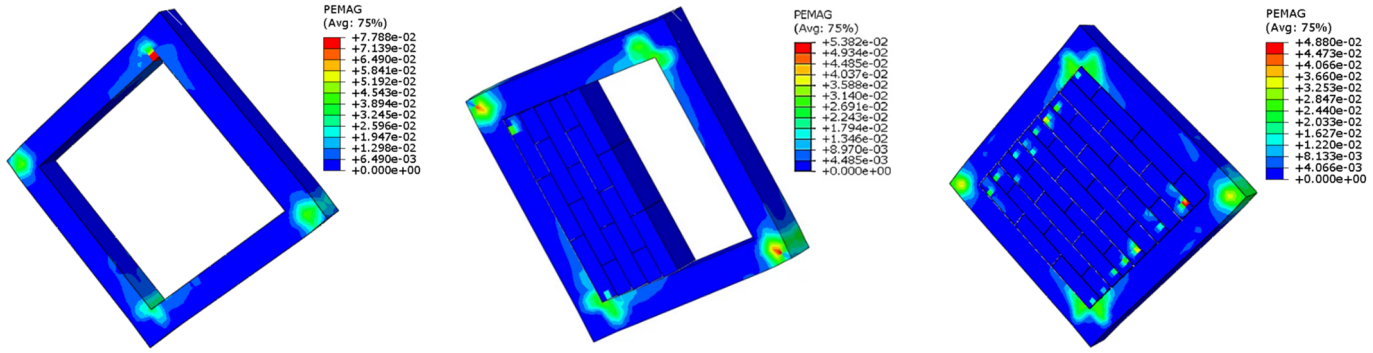

(**a**) (**b**) (**c**)

Figure 14. Damage locations after FEM analysis: (**a**) P1-00, (**b**) P1-50 and (**c**) P3-100.

4. Discussion: Engineering Background, Practical Value, and Limitations

The results of this study contribute to the ongoing effort to integrate sustainable materials into seismic-resistant structural systems. The reuse of intact solid clay bricks from demolition waste addresses both environmental and engineering challenges by reducing landfill disposal and providing a readily available infill material for reinforced concrete (RC) frames. This approach aligns with circular-construction principles and offers a low-energy alternative to producing new masonry units. Cross-comparison with recent experimental programs supports these interpretations. Infilled, properly connected frames exhibit substantial stiffness and strength gains [28], whereas construction gaps or poor contact can eliminate much of this benefit [31] and alter failure modes toward column shear. The results of this study fall within the range of responses reported for infilled RC frames, showing comparable magnitudes and consistent behavioral trends.

From an engineering standpoint, the findings demonstrate that recycled solid-brick infills can restore and even enhance the lateral stiffness and strength of existing RC frames. The observed increase in diagonal shear strength (≈149%) confirms the potential of these infills to improve initial stiffness and delay the onset of soft-story mechanisms during seismic excitation. However, the accompanying reduction in ductility (≈40%) highlights the need for careful design of infill continuity and boundary conditions to avoid brittle failure. For moderate seismic zones, partial or discontinuous infills could represent an optimal balance between stiffness and ductility, enhancing energy dissipation without inducing premature cracking.

In terms of practical value, the research outcomes support the use of reclaimed bricks in low- and mid-rise structural applications, non-structural partitions, and retrofitting projects where moderate shear resistance and improved serviceability are desired. The direct reuse of bricks, without reprocessing, substantially reduces construction costs, material waste, and embodied carbon, making it a viable strategy for sustainable urban development. These findings suggest that recycled brick infills can be effectively incorporated into low-rise residential, educational, and public buildings, or used to retrofit existing RC frames in moderate seismic zones, where balanced stiffness and ductility contribute to improved overall resilience.

Beyond their structural function, the reuse of recycled masonry infills contributes meaningfully to sustainable and resilient construction. By lowering the demand for newly fired clay bricks—one of the most energy-intensive conventional materials—this approach reduces embodied energy and CO_2 emissions while diverting demolition debris from landfills. Integrating such low-carbon materials into seismic-resistant systems supports Sustainable Development Goal 11 (“Sustainable Cities and Communities”) and strengthens the link between structural performance and environmental responsibility.

Despite these benefits, several limitations should be noted. The experimental program was limited to monotonic diagonal compression and did not include cyclic loading, which would provide a fuller assessment of energy dissipation and post-cracking behavior. Moreover, only one large-scale specimen per configuration was tested, constraining statistical generalization. The finite element model, while capturing global response accurately, simplifies masonry interface behavior and does not simulate local crack propagation at the joint scale. Future work should therefore extend testing to cyclic regimes, incorporate multiple replicates for variance analysis, and explore meso-scale or digital volume correlation–based calibration of interface laws to enhance predictive accuracy.

Overall, this study provides both proof of concept and engineering validation for using recycled masonry infills in sustainable seismic design, offering a foundation for the development of future design guidelines and performance-based assessment frameworks.

5. Significance of the Study

This research demonstrates that recycled solid-brick masonry infills can enhance the lateral strength and stiffness of reinforced concrete (RC) frames without extensive material reprocessing. The observed 149% increase in diagonal shear strength confirms their capacity to act as passive energy-dissipating components, improving seismic resilience by delaying soft-story mechanisms and reducing interstory drifts. From an environmental standpoint, reusing intact masonry units eliminates the need for energy-intensive brick firing and diverts demolition waste from landfills, contributing to lower embodied CO_2 emissions and circular-economy objectives. The resulting systems exhibit a favorable balance between strength and controlled ductility, allowing energy dissipation without full structural collapse. This synergy between sustainability and seismic performance highlights the dual structural–environmental advantage of recycled masonry and aligns with Sustainable Development Goal 11 (Sustainable Cities and Communities), offering practical insight for retrofitting and new low-rise construction in earthquake-prone regions.

6. Conclusions

The experimental and numerical results demonstrate the feasibility of reusing solid clay bricks from demolished structures as effective masonry infills and load-bearing elements. Based on the outcomes of this study, the following main conclusions can be drawn:

- Recycled solid-brick infills significantly enhanced the in-plane capacity of reinforced concrete (RC) frames, leading to an increase of approximately 149% in diagonal shear strength compared with the bare frame, while maintaining acceptable deformation compatibility.
- A clear trade-off between strength and ductility was observed: fully infilled frames exhibited the highest stiffness and strength but reduced ductility by around 40%, indicating that partial or discontinuous infills may offer a balanced seismic response.
- The finite element model, based on the Concrete Damaged Plasticity (CDP) formulation with cohesive interface contact, accurately reproduced the experimental load–displacement behavior with deviations in peak load below 8%, confirming its adequacy for macro-scale structural analysis.
- The reuse of intact solid bricks presents both structural and environmental advantages, reducing construction waste and embodied CO_2 emissions while enhancing seismic resilience. The approach supports circular-construction practices and aligns with Sustainable Development Goal 11 (Sustainable Cities and Communities).

These findings underline the innovative aspect of directly reusing masonry units without reprocessing, providing a practical pathway toward sustainable and resilient construction in regions with high demolition waste generation.

Author Contributions: Conceptualization, E.L. (Erion Luga), E.L. (Ervis Lika) and E.M.; methodology, E.L. (Erion Luga) and E.M.; software, E.T.; validation, M.C. and E.L. (Erion Luga); formal analysis, E.L. (Ervis Lika) and M.C.; investigation, E.L. (Erion Luga) and E.T.; resources, E.L. (Ervis Lika) and E.P.; data curation, M.C.; writing—original draft preparation, E.M.; writing—review and editing, M.C.; visualization, E.L. (Erion Luga); supervision, E.M. All authors have read and agreed to the published version of the manuscript.

Funding: This research received no external funding.

Data Availability Statement: The data presented in this study are available on request from the corresponding author.

Conflicts of Interest: Author Ervis Lika is employed by the Risi Construction Company. The remaining authors declare that the research was conducted in the absence of any commercial or financial relationships that could be construed as a potential conflict of interest.

References

1. Seco, A.; Omer, J.; Marcelino, S.; Espuelas, S.; Prieto, E. Sustainable unfired bricks manufacturing from construction and demolition wastes. *Constr. Build. Mater.* **2018**, *167*, 154–165. [CrossRef]
2. Dos Reis, G.S.; Cazacliu, B.G.; Cothenet, A.; Poullain, P.; Wilhelm, M.; Sampaio, C.H.; Lima, E.C.; Ambros, W.; Torrenti, J.-M. Fabrication, microstructure, and properties of fired clay bricks using construction and demolition waste sludge as the main additive. *J. Clean. Prod.* **2020**, *258*, 120733. [CrossRef]
3. Hopkinson, P.; Chen, H.M.; Zhou, K.; Wang, Y.; Lam, D. Recovery and reuse of structural products from end-of-life buildings. *Proc. Inst. Civ. Eng.—Eng. Sustain.* **2018**, *172*, 119–128. [CrossRef]
4. Richardson, H.G.; Richardson, E.M. *The English Brickmaker: A History of Brickmaking and Brick Building in England from the Roman Times to the Present Day*; Osprey Publishing: London, UK, 1961.
5. Erdem, I.; Akyuz, U. Analytical investigation of lateral strength of masonry infilled RC frames retrofitted with CFRP. *J. Perform. Constr. Facil.* **2010**, *24*, 302–310. [CrossRef]
6. Zhai, C.; Wang, X.; Kong, J.; Li, S.; Xie, L. Numerical simulation of masonry-infilled RC frames using XFEM. *J. Struct. Eng.* **2017**, *143*, 04017144. [CrossRef]
7. Hammoudah, S.M.W.; Chaudhary, M.T.A.; Essawy, A.S. Analytical and parametric study on masonry infilled reinforced concrete frames using finite element method. *Adv. Struct. Eng.* **2017**, *20*, 1891–1906. [CrossRef]
8. Tanjung, J.; Mohamed Nazri, F.; Hayati, Y. A simple strengthening method for preventing collapse of vulnerable masonry infills. *Buildings* **2022**, *12*, 1496. [CrossRef]
9. Cumhur, A.; Altundal, A.; Aykac, S.; Aykac, B. Strengthening of hollow brick infill walls with expanded steel plates. *Earthq. Struct.* **2016**, *11*, 887–904. [CrossRef]
10. Mutsuddy, R.; Das, S.S.; Majumder, S.N. Influence of nylon fiber on the response of carbon fiber reinforced polymer (CFRP)-retrofitted RC frame under cyclic load. *Asian J. Civ. Eng.* **2024**, *25*, 3011–3024. [CrossRef]
11. Dehghani, A.; Nateghi-Alahi, F.; Fischer, G. Engineered cementitious composites for strengthening masonry infilled reinforced concrete frames. *Eng. Struct.* **2015**, *105*, 197–208. [CrossRef]
12. Selvaraj, B.R.; Rai, D.C. Effect of in-plane damage on out-of-plane response of FRCM strengthened masonry infilled RC frames. *J. Compos. Constr.* **2022**, *26*, 04022070. [CrossRef]
13. Lu, X.; Zha, S. Full-scale experimental investigation of the in-plane seismic performance of a novel resilient infill wall. *Eng. Struct.* **2021**, *232*, 111826. [CrossRef]
14. Chen, Z.; Zhou, Y.; Kinoshita, T.; DeJong, M.J. Distinct element modeling of the in-plane and out-of-plane response of ordinary and innovative masonry infill walls. *Structures* **2023**, *50*, 1447–1460. [CrossRef]
15. Guettala, S.; Khelaifia, A.; Abdesselam, I.; Chebili, R.; Guettala, S. Assessment of seismic fragility of 3D reinforced concrete structures with masonry infill walls under different distribution arrangements. *Asian J. Civ. Eng.* **2024**, *25*, 5525–5532. [CrossRef]
16. Zare, A.R.; Vosoughi, A.R.; Najafgholipour, M.A. Steel honeycomb elements for improving the seismic performance of moment-resisting frames with masonry infills. *Structures* **2023**, *57*, 105237. [CrossRef]
17. Stazi, F.; Serpilli, M.; Maracchini, G.; Pavone, A. An experimental and numerical study on CLT panels used as infill shear walls for RC buildings retrofit. *Constr. Build. Mater.* **2019**, *211*, 605–616. [CrossRef]
18. Furtado, A.; Rodrigues, H.; Arêde, A.; Varum, H. Experimental tests on strengthening strategies for masonry infill walls: A literature review. *Constr. Build. Mater.* **2020**, *263*, 120520. [CrossRef]
19. Ricci, P.; Di Domenico, M.; Verderame, G.M. Experimental assessment of the in-plane/out-of-plane interaction in unreinforced masonry infill walls. *Eng. Struct.* **2018**, *173*, 960–978. [CrossRef]

20. Xue, J.; Huang, X.; Luo, Z.; Gao, L. Experimental and numerical studies on the frame-infill interaction in steel-reinforced recycled concrete frames. *Steel Compos. Struct.* **2016**, *20*, 1391–1409. [CrossRef]
21. *E519-02*; Test Method for Diagonal Tension (Shear) in Masonry Assemblages. C15 Committee: West Conshohocken, PA, USA, 2017. [CrossRef]
22. *BS 4449:2005+A3:2016*; Steel for the Reinforcement of Concrete—Weldable Reinforcing Steel—Bar, Coil and Decoiled Product—Specification. BSI: London, UK, 2016.
23. *EN 1992-1-1*; Eurocode 2: Design of Concrete Structures—Part 1-1: General Rules and Rules for Buildings. European Committee for Standardization (CEN): Brussels, Belgium, 2004.
24. *EN 206-1*; Concrete—Specification, Performance, Production, and Conformity. European Committee for Standardization (CEN): Brussels, Belgium, 2000.
25. *EN 771-1*; Specification for Masonry Units—Part 1: Clay Masonry Units. European Committee for Standardization (CEN): Brussels, Belgium, 2011.
26. *EN 196-1*; Methods of Testing Cement—Part 1: Determination of Strength. European Committee for Standardization (CEN): Brussels, Belgium, 2016.
27. Elkady, A. *ABAQUS CDP Generator*, Version v23.04; Zenodo: Geneva, Switzerland, 2023. [CrossRef]
28. Nasiri, E.; Liu, Y. Effect of prior in-plane damage on the out-of-plane performance of concrete masonry infills. *Eng. Struct.* **2020**, *222*, 111149. [CrossRef]
29. Lourenço, P. Computational Strategies for Masonry Structures. Ph.D. Thesis, Delft University of Technology, Delft, The Netherlands, 1996.
30. Simulia. *ABAQUS Analysis User's Manual*; Hibbitt, Karlsson, and Sorenson: Pawtucket, RI, USA, 2024.
31. Kim, M.; Yu, E. Experimental Study on Lateral-Load-Resisting Capacity of Masonry-Infilled Reinforced Concrete Frames. *Appl. Sci.* **2021**, *11*, 9950. [CrossRef]
32. Wang, C.; Guo, J.; Wang, X.; Zhang, Y.; Ma, Z. Dynamic mechanical properties and damage constitutive model of high-toughness recycled aggregate concrete under high strain rate impact loads. *Constr. Build. Mater.* **2025**, *400*, 133157. [CrossRef]
33. Grubišić, M.; Šipoš, T.K.; Grubišić, A.; Pervan, B. Testing of damaged single-bay reinforced concrete frames strengthened with masonry infill walls. *Buildings* **2023**, *13*, 1021. [CrossRef]

Disclaimer/Publisher's Note: The statements, opinions and data contained in all publications are solely those of the individual author(s) and contributor(s) and not of MDPI and/or the editor(s). MDPI and/or the editor(s) disclaim responsibility for any injury to people or property resulting from any ideas, methods, instructions or products referred to in the content.